PERGAMON

International Journal of Plasticity 19 (2003) 625–646

INTERNATIONAL JOURNAL OF Plasticity

www.elsevier.com/locate/ijplas

Anisotropic viscous behavior of sheet molding compounds (SMC) during compression molding

P. Dumont, L. Orgéas*, S. Le Corre, D. Favier

Laboratoire Sols, Solides, Structures, CNRS, Université Joseph Fourier, Institut National Polytechnique de Grenoble, BP 53, 38041 Grenoble Cedex 9, France

Received in final revised form 7 November 2001

Abstract

To improve the knowledge on the rheology of sheet molding compounds (SMC) during compression molding, a specific rheometer was designed, allowing to perform homogeneous experiments on SMC specimen under various mechanical loading, strain rates and fiber contents. Results gained during experiments underlined the key role played both by the strain rate and the fiber content. A viscous and transversely isotropic model was then proposed and used to fit stress levels recorded during the experiments. This model that requires few constitutive parameters rather well describes the main features of SMC rheology.

Keywords: B. Anisotropic viscous material; B. Fiber-reinforced composite material; B. Constitutive behavior; B. Sheet molding compounds (SMC); C. Mechanical testing, C. Rheometer

1. Introduction

Sheet molding compounds (SMC) consist mainly of a *paste* reinforced with *short glass fibers*. The paste is generally a polyester resin filled with calcium carbonate and other additives, whereas glass fibers are initially randomly oriented in the plane of the sheets and make up for about 15–30% of the weight fraction of industrial compounds. The industrial processing technique of SMC parts, i.e. compression molding, consists first in a rapid squeezing of a set of cold (≈25 °C) stacked charges of SMC in a hot mold (≈150 °C) at a closure speed of ≈1–10 mm s^{-1}. This stage is followed by a curing period of about 60–120 s in the closed mold. Due to both their specific mechanical and electrical properties and their cost efficient processing, these materials are widely used by the automotive industry and by the electrical industry to produce rigid and lightweight parts.

* Corresponding author. Tel.: +33-4-76-82-70-73; fax : +33-4-76-82-70-43.
E-mail address: laurent.orgeas@hmg.inpg.fr (L. Orgéas).

0749-6419/03/$ - see front matter
PII: S0749-6419(01)00077-8

So far many works have been performed to analyze mechanisms of SMC flow during compression molding (Marker and Ford, 1977; Silva-Nieto et al., 1980; Barone and Caulk, 1985; Castro and Griffith, 1989; Xu et al., 1993). In contrast with the high number of experimental studies devoted to the process, references to the rheological properties of these compounds during the compression stage are quite scarce and incomplete (Silva-Nieto et al., 1981; Lee et al., 1981; Michaeli et al., 1990; Kim et al., 1992, 1997; Lin et al., 1997; Lin and Weng, 1999). A better knowledge of their properties would contribute to the improvement of rheological models implemented in simulation software (Lee et al., 1984; Barone and Caulk, 1986; Castro and Tomlinson, 1990). Such a lack can be largely explained by the inability of usual rheometers to characterize these materials. Indeed, in order to obtain meaningful results, the dimensions of the tested samples have to be chosen in proportion to the size of the fibers. On the one hand, this leads to design non-usual rheometers. On the other hand, this implies to use a powerful testing machine to carry out tests on large samples.

Silva-Nieto et al. (1981) first studied the SMC behavior by squeezing some cylindrical samples (40 mm in diameter) between parallel and non-lubricated plates. Only one glass fiber weight fraction of 25% was tested at room temperature and at constant plate-closure speeds ranging from 0.016 to 0.8 mm s^{-1}. The applied force was found to be an increasing function of the plate closure speed. However, no quantitative results could be drawn from their work for several reasons. Firstly, the dimensions of fibers were not mentioned, so that it is impossible to check if the samples' diameter was sufficiently large compared with the fibers' length. Secondly, their experiments involved heterogeneous stress state (combined compression-shear stress states with spatial gradient) and were analyzed assuming an incompressible and isotropic behavior (Scott, 1931). The isotropy assumption is not consistent with the anisotropic microstructure of SMC, since fibers are randomly spread in a loosely woven fiber structure parallel to the plane of the sheets. At last, their studied closure speed range was far below from that one encountered during compression molding.

Among the former analyses, Lee et al. (1981) had the most rigorous approach. Tested samples were made either of paste or SMC (glass fiber weight fraction of 10 and 30% and fibers' length of 12.5 and 25 mm). An extensive number of shear tests (using usual rheometer) were performed with paste, whose steady state non-Newtonian viscosity was found to follow a Carreau type function of the applied shear rate and an Arrhenius type function of the temperature. SMC behavior was mainly studied by performing simple compression creeping tests (constant applied force) on cylindrical samples (200 mm in diameter) squeezed between lubricated plates were also achieved. The compressive viscosity of SMC was found to be strain rate dependent. A strong influence of the fiber content on the compressive viscosity of SMC was also recorded and was correlated with a Batchelor type approach (Batchelor, 1970). However, despite the precious qualitative tendencies underlined by this work, no real quantitative data were drawn and no rheological model was proposed to describe the behavior of SMC. Because of some experimental difficulties, few shear and tensile tests could be performed on SMC.

More recently, Lin et al. (1997) and Lin and Weng (1999) performed simple compression and plane strain compression tests with 25% fiber volume fraction SMC (fiber length of 25.4 mm). For simple compression tests, cylindrical samples of

diameter 150 mm made of stacked sheets up to a thickness of 8 mm were used. For plane strain compression tests, rectangular prisms ($120\times44\times8$ mm^3) were deformed through a rectangular mould (120 mm long and 44 mm wide). In both cases, the axial strain rates, kept constant during loading, were varied between 0.2 and 1 s^{-1}. The results of these two sets of experiments were used to determine some of the parameters of a rheological model initially proposed by Kim et al. to model the anisotropic, incompressible and non-Newtonian viscous behavior of SMC (Kim et al., 1992). This model assumes a viscoplastic potential, function of an equivalent stress. The equivalent stress is similar to the quadratic Hill's yield stress reduced to the case of planar isotropy (Hill, 1950), and involves three anisotropic parameters. Experimental results showed that the equivalent stress was a non-linear function of the imposed strain-rate, and enabled to determine two of the three anisotropic parameters, the last required parameter being estimated with a Batchelor type approach. However, in Lin et al.'s work, only one fiber volume fraction was studied, and a very small strain rate range was analyzed (0.2–1 s^{-1}). At last, as it will be pointed out in the present paper, the identification procedure they used may yield to erroneous modeling.

It appears from the previous discussion that a wider experimental database is needed to better understand and model the anisotropic rheological behavior of SMC. This database must be obtained for process representative mechanical loading, fiber contents and temperatures. This is the main objective of our contribution. In a previous paper (Le Corre et al., in press), the rheological properties of an industrial SMC was studied in simple compression (*sc*) and shear (*s*) at various strain rates (10^{-3}–10 s^{-1}), various fiber volume fraction (0–23%) and various temperature (296–343 K). In the present paper, new results of simple compression experiments at room temperature are presented. Moreover, original plane strain compression (*ps*) experiments performed on the same SMC are presented. Denoting $\mathbf{e}_3$ the perpendicular direction to the plane of the sheets, the stress $\boldsymbol{\sigma}$, strain $\boldsymbol{\varepsilon}$ and strain rate $\mathbf{D}$ tensors for simple compression and plane strain compression are respectively given in the Cartesian reference frame ($\mathbf{e}_1$, $\mathbf{e}_2$, $\mathbf{e}_3$) by the following sets:

$$\boldsymbol{\sigma}=\begin{bmatrix}0&0&0\\0&0&0\\0&0&\sigma_{33}\end{bmatrix},\quad \boldsymbol{\varepsilon}=\begin{bmatrix}\varepsilon_{11sc}&0&0\\0&\varepsilon_{22sc}&0\\0&0&\varepsilon_{33sc}\end{bmatrix},\quad \mathbf{D}=\begin{bmatrix}D_{11sc}&0&0\\0&D_{22sc}&0\\0&0&D_{33sc}\end{bmatrix} \tag{1}$$

$$\boldsymbol{\sigma}=\begin{bmatrix}0&0&0\\0&\sigma_{22ps}&0\\0&0&\sigma_{33ps}\end{bmatrix},\quad \boldsymbol{\varepsilon}=\begin{bmatrix}\varepsilon_{11ps}&0&0\\0&0&0\\0&0&\varepsilon_{33ps}\end{bmatrix},\quad \mathbf{D}=\begin{bmatrix}D_{11ps}&0&0\\0&0&0\\0&0&D_{33ps}\end{bmatrix} \tag{2}$$

For that purpose, a specific rheometer was designed (Le Corre et al., in press). Using three specimen shapes and three different configurations, this rheometer

allows to perform shear tests, compression tests and plane strain compression tests. In that last case, an original measurement of the transverse force F_{2ps} was achieved to estimate the transverse stress σ_{22ps} (Section 2). Experimental results (Section 3) first raise the problem of the specimen dimensions with respect to the fiber length. Results also underline the non-linear strain rate influence on stress levels and the role of fiber volume fraction on the SMC behavior. In Section 4, a set of constitutive equations taking into account viscous effects and anisotropy is proposed to model the rheological behavior of the studied SMC. Based on the present experimental data, the constitutive parameters of such a model are determined (Section 5). In particular, two methods of determination are examined and discussed.

2. Materials, equipment and experimental procedure

2.1. Materials

The tested SMC consist of polyester based paste reinforced with 25 mm long glass bundles (composed of approximately one hundred small glass fibers having a diameter of 15 μm). It was supplied by Mecelec Composites And Recyclage (France). As listed in Table 1, the main ingredients of the paste are typical of a low profile formulation. Six different glass fiber weight fractions were studied, i.e. 0, 5, 10, 15, 20 and 25%. These weight fractions correspond to glass fiber volume fractions ϕ of 0, 3.5, 7.1, 10.8, 14.7 and 18.8%, respectively. The tested samples were made of layers cut off from some sheets of SMC. Due to their industrial processing, these sheets display a rather irregular thickness and wavy surface. For instance, a 120×120 mm^2 layer had an average thickness h_0 of 2.7 mm that varied in a range Δh_0 of $\pm$ 0.25 mm. This will affect the accuracy of our results (Section 2.3).

2.2. Experimental apparatus and procedure

A rheometer was designed to carry out simple compression tests and plane strain compression tests on SMC specimens. It was mounted in a 100 kN hydraulic MTS press with a maximum cross-head velocity of 1 m s^{-1}.

Simple compression tests were performed on cylindrical samples of initial thickness h_0 and initial diameter D_0 made up of three circular stacked layers of SMC. As

Table 1
Ingredients of the paste

Ingredient	Wt.%
Polyester resin	19.60
Styrene	1.56
Catalyst + inhibiter	0.56
ZnSt	1.31
LP additive	13.07
M additive	0.98
Magnesia	0.85
$CaCO_3$	62.07

shown in Fig. 1a, samples were squeezed between two polished plates (400 mm in diameter) made of aluminum alloy and coated with silicone grease. Five different initial diameters were tested, i.e. 50, 75, 100, 160 and 200 mm. During the experiments, the axial force F_{3sc} and the instantaneous height h of the sample were on-line collected. These measurements together with the initial dimensions of the sample were used to determine the axial stress σ_{33sc}, the axial strain ε_{33sc} and the axial strain rate D_{33sc} assuming SMC are incompressible materials:

$$\sigma_{33sc} = \frac{4}{\pi}\frac{F_{3sc}}{D_0^2}\frac{h}{h_0}, \qquad \varepsilon_{33sc} = \ln\left(\frac{h}{h_0}\right), \qquad D_{33sc} = \frac{\dot{h}}{h} \tag{3}$$

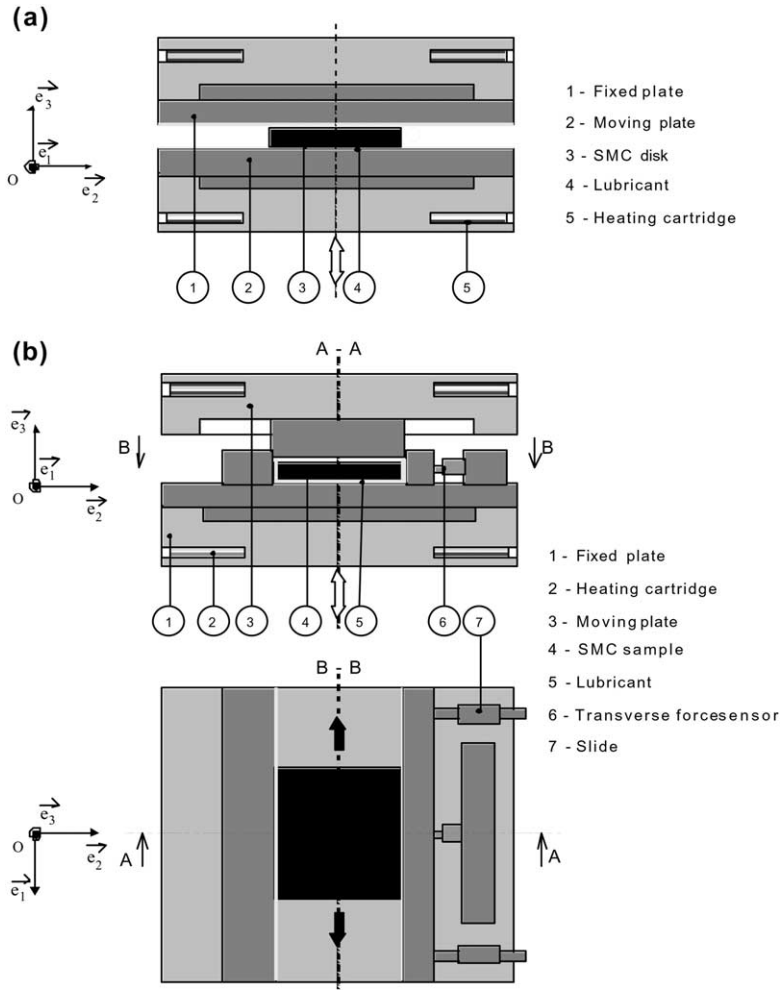

Fig. 1. SMC rheometer, (a) simple compression configuration and (b) plane strain compression configuration.

All simple compression tests were performed at room temperature (296 K) and at constant axial strain rates D_{33sc} ranging from 10^{-3} to 1 s^{-1}. The maximum axial strain ε_{33sc} could easily reach 0.7, which corresponded to a 75% reduction of the sample thickness. This rate is usually reached during the industrial compression process.

As depicted in the simplified scheme of Fig. 1b, the rheometer was modified to obtain a plane strain compression loading. This device is similar to the one used in a recent study (Lin et al., 1997). However, in the present work, both the axial force F_{3ps} and the transverse force F_{2ps} exerted on the sample were measured (upper view of the rheometer in Fig. 1b) to better estimate the stress state during experiments. Surfaces of this modular apparatus (maximum length $x_{1\max}=400$ mm and maximum height $x_{3\max}=30$ mm) in contact with the sample were polished and coated with a thin layer of silicone grease like for simple compression tests. To measure the transverse force, a force transducer was fastened behind one side of the channel mounted in a slide, as shown in Fig. 1b. Samples of different widths l_0 (in the x_2 direction) could be tested, i.e. 80, 100, 120 and 160 mm. Tests were performed on rectangular prisms (length L_0, width l_0, height h_0) made of three sheets. In this work, the initial length L_0 varied from 40 to 160 mm, whereas the initial width l_0 was kept constant (120 mm). In addition to the forces F_{3ps} and F_{2ps}, the instantaneous height h of the samples was recorded during the experiments.

Assuming that SMC are incompressible, these measurements provided the axial and transverse stresses, namely σ_{33ps} and σ_{22ps}, the axial strain ε_{33ps} and the axial strain rate D_{33ps}:

$$\sigma_{33ps}=\frac{F_{3ps}\ h}{L_0\ l_0\ h_0},\qquad \sigma_{22ps}=\frac{F_{2ps}}{l_0h_0},\qquad \varepsilon_{33ps}=\ln\left(\frac{h}{h_0}\right),\qquad D_{33ps}=\frac{\dot{h}}{h} \tag{4}$$

Each test was carried out at room temperature (296 K) and at constant axial strain rates ranging from 10^{-3} to 1 s^{-1}. During these experiments, the maximum axial strain ε_{33ps} reached 0.7.

2.3. Influence of experimental conditions on tests

The general aspect of the stress-strain curves obtained for simple compression and plane strain compression tests is depicted in Fig. 2. Three stages are systematically observed in the variation of the axial stress σ_{33sc} of simple compression as a function of ε_{33sc} (Fig. 2a). The first stage corresponds to a sharp increase of the stress to a threshold σ_{33sct}. Then, in a second stage, for strain values ranged from 0.2 to 0.4, the level of stress remains approximately constant. In the last stage of compression, a smooth increase is observed. As evident in Fig. 2b, the variation of the σ_{33ps}–ε_{33ps} obtained for plane strain compression tests and σ_{22ps}–ε_{33ps} curves follow the same pattern as the σ_{33sc}–ε_{33sc} one. Thus, threshold stresses were defined for plane strain compression experiments, i.e. the axial stress σ_{33pst} and the transverse stress σ_{22pst}. In the following sections, results and discussion concerning stresses will be given in terms of these threshold stresses (σ_{33sct}, σ_{33pst} and σ_{22pst}).

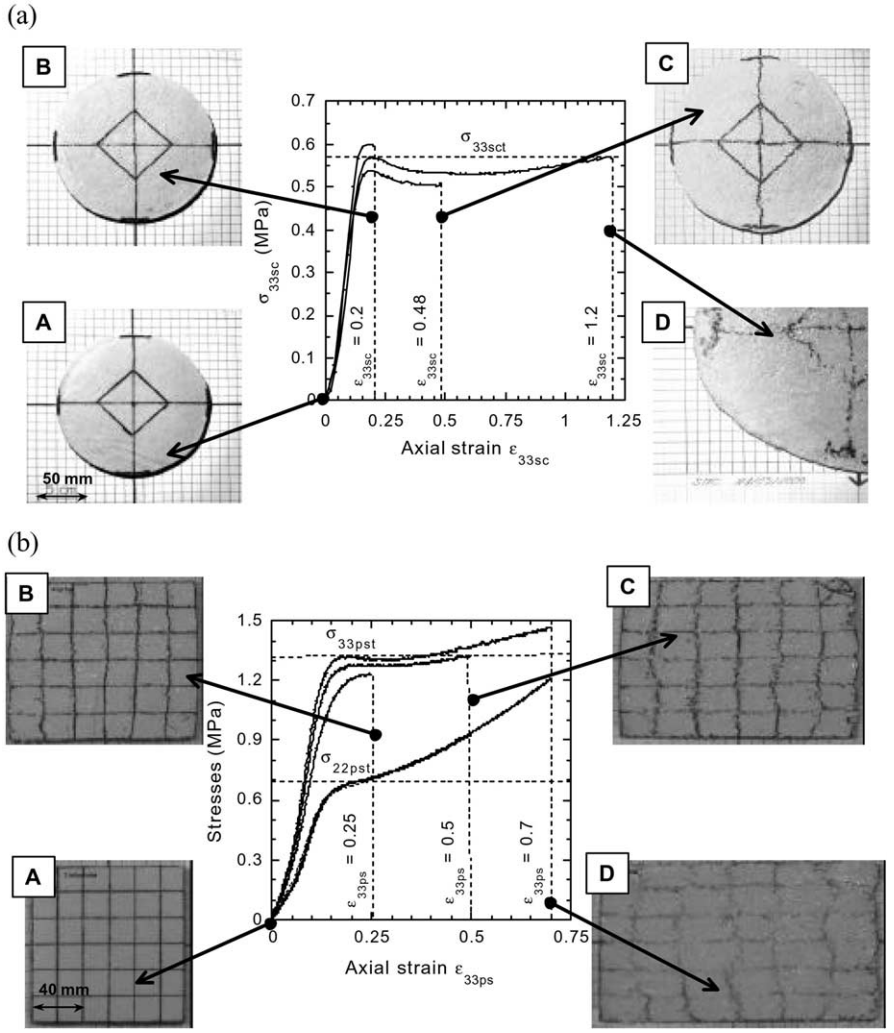

Fig. 2. Typical (a) simple compression experiments ($\phi = 14.7\%$, $D_{33sc} = 0.01\,s^{-1}$) and (b) plane strain compression experiments ($\phi = 10.8\%$, $D_{33ps} = 0.01\,s^{-1}$).

Several preliminary tests were performed with SMC samples to determine the optimal conditions providing homogeneous stress–strain state and reproducible results.

In order to display a possible friction effect on the measurements of the axial stress σ_{33sct}, many lubricated paste samples of different initial diameters D_0 ranging from 50 to 200 mm and different heights h_0 ranging from 6 mm to 16 mm, were submitted to simple compression at constant axial strain rate $D_{33sc} = 0.1\ s^{-1}$. Similarly, rectangular prisms made of paste, i.e. L_0 ranging from 80 to 172 mm and h_0 ranging from 6 to 16 mm, were submitted to plane strain compression at $D_{33ps} = 0.1\ s^{-1}$. In

both cases, it was clearly established that the level of the stresses did not depend on the dimensions of the paste samples. As a consequence, friction effects between the molds and the samples were proved to be negligible.

The assumptions of frictionless and homogeneous kinematics of simple compression [see Eq. (1)] and plane strain compression [see Eq. (2)] were also checked on SMC samples. For that purpose plane strain compression tests were performed with lubricated and sufficiently large SMC samples (see Section 3.1) in the shape of rectangular prisms ($L_0 \times l_0 \times h_0 = 120 \times 120 \times 8$ mm^3). Whatever the imposed strain rate D_{33ps} and the initial fiber volume fraction ϕ were, it was observed that the initial rectangular shape of each specimen was fairly well kept during flow at various stages of axial strains ε_{33ps}. As shown in Fig. 2b, the initial square shape A of the samples extended uniformly to a rectangular shape (B, C) even up to a large strain $\varepsilon_{33ps} = 0.7$ (see deformed sample D). No fountain-like flow was observed in the (x_1, x_2) plane: possible friction effect between the specimen and the vertical sides of the mold ($x_1 = \pm l_0/2$) were then negligible. The highlighted marks located at the free surface of the samples ($x_1 = \pm L_0/2$) of the initial sample A remained at the boundaries of the deformed samples ($x_1 = \pm L/2$), as evident for samples B, C and D. Moreover, it was visually checked that vertical lines initially drawn on the sides ($x_2 = \pm l_0/2$) of the samples remained vertical after deformation. A similar analysis was performed on large SMC samples ($D_0 = 160$ mm, $h_0 = 8$ mm) deformed under simple compression: whatever the imposed strain rate D_{33sc} and the initial fiber volume fraction ϕ were, the flow pattern remained homogeneous at the sample scale up to very large axial strain states, as shown in Fig. 2a. As a result it was reasonable to consider that the strain state in sufficiently large and lubricated samples was "globally" homogeneous in the case of simple compression as well as in the case of plane strain compression tests.

Even under such "optimal" testing conditions, a rather poor accuracy of $\pm 20\%$ on stresses measurements was systematically recorded. Such a high value is commonly encountered in the study of SMC rheology (Silva-Nieto et al., 1981; Kim et al., 1997; Le Corre et al. in press). Results are certainly affected by the rather irregular initial thickness h_0 of the samples ($\Delta h_0/h_0 \approx \pm 10\%$), the inaccuracy of L_0, l_0 or D_0 ($\Delta L_0/L_0 \approx \Delta l_0/l_0 \approx \Delta D_0/D_0 \approx \pm 2\%$) and the error on the strain rate D_{33} ($\Delta D_{33}/D_{33} \approx \pm 5\%$).

3. Experimental results

3.1. Determination of the scale at which the deformation is homogeneous

The homogeneity of SMC samples ($\phi \neq 0$) deformation, discussed in the former section, was proved only in the case of sufficiently large SMC samples. However, a closer analysis of the deformed grids obtained in plane strain compression experiments (Fig. 2b) shows that kinematics is locally strongly heterogeneous, due to local motion of fibers. Such a feature was carefully investigated by making use of the grid drawn on the surfaces of the samples (Fig. 2b). The strain ε_{11ps} of horizontal segments was calculated:

$$\varepsilon_{11ps} = \ln\left(\frac{l_f}{l_i}\right) \tag{5}$$

where l_i and l_f are the initial and elongated lengths of the segments. These segments were picked at a different location on the surface of the samples and their initial length ranged from 20 to 120 mm. The influence of l_i on ε_{11ps} is given in Fig. 3a in the case of the deformed sample B displayed in Fig. 2b. As it is clearly illustrated in Fig. 3a, the lower the initial length l_i, the higher the scattering of ε_{11ps} is. On the contrary, if l_i is larger than 100 mm, the scattering of ε_{11ps} is fairly small, and the segment location on the surfaces of the sample no longer has any influence on ε_{11ps}. A similar analysis was carried out using simple compression samples. In order that the strain ε_{11sc} did not depend on where the segments were picked, the initial diameter D_0 had to be larger than 100 mm. Hence, we concluded that the strain field was homogeneous from a macroscopic point of view if the initial dimensions L_0 in plane strain compression and D_0 in compression were larger than 100 mm.

Similar trends were found in the analysis of stress states. SMC disks with initial diameter D_0 ranging from 50 to 200 mm were submitted to simple compression at a same axial strain rate D_{33sc}. Fig. 3b first shows that an asymptotic stress value is reached for initial diameter larger than 100 mm. Furthermore, as depicted in Fig. 3b, a rather good reproducibility of the measurements of the axial stress σ_{33sct} was obtained for cylindrical samples having an initial diameter larger than 100 mm. Similarly, plane strain compression tests were also performed with SMC samples in the shape of rectangular prisms ($L_0 = 20$ to 120 mm, $l_0 = 120$ mm). They showed that identical measurements of stresses σ_{33pst} and σ_{22pst} were obtained if the initial length was larger than 100 mm.

Results established for stresses coincide with those obtained for strains. They show that the dimensions of samples had to be chosen in proportion to the size of the fibers. As a consequence, all simple compression results presented in the following sections were obtained from SMC disks having an initial diameter D_0 of 160 mm. The plane strain compression results were obtained for prismatic samples having a sufficiently large length L_0 of 120 mm and a width l_0 of 120 mm.

3.2. Influence of strain rates

Fig. 4 contains typical results showing the influence of the strain rate D_{33} on the axial stress σ_{33t} (t holds for threshold) obtained from simple compression tests (in this case, consider σ_{33sct} and D_{33sc}) and from plane strain compression ones (consider σ_{33pst} and D_{33ps}), at different fiber volume fractions. The symbols represent the experimental points and the full lines represent power-law functions used to fit experimental data. In the case of simple compression experiments (Fig. 4a), one finds:

$$\sigma_{33sct} = \eta^{\phi}_{33sc}\left(\frac{D_{33sc}}{D_0}\right)^{n^{\phi}-1} D_{33sc} \tag{6}$$

In the last equation, η^{ϕ}_{33sc} is a viscosity defined for a reference axial strain rate $D_0 = 1\ \mathrm{s}^{-1}$ and n^{ϕ} is the power-law exponent (strain rate sensitivity). For a given fiber

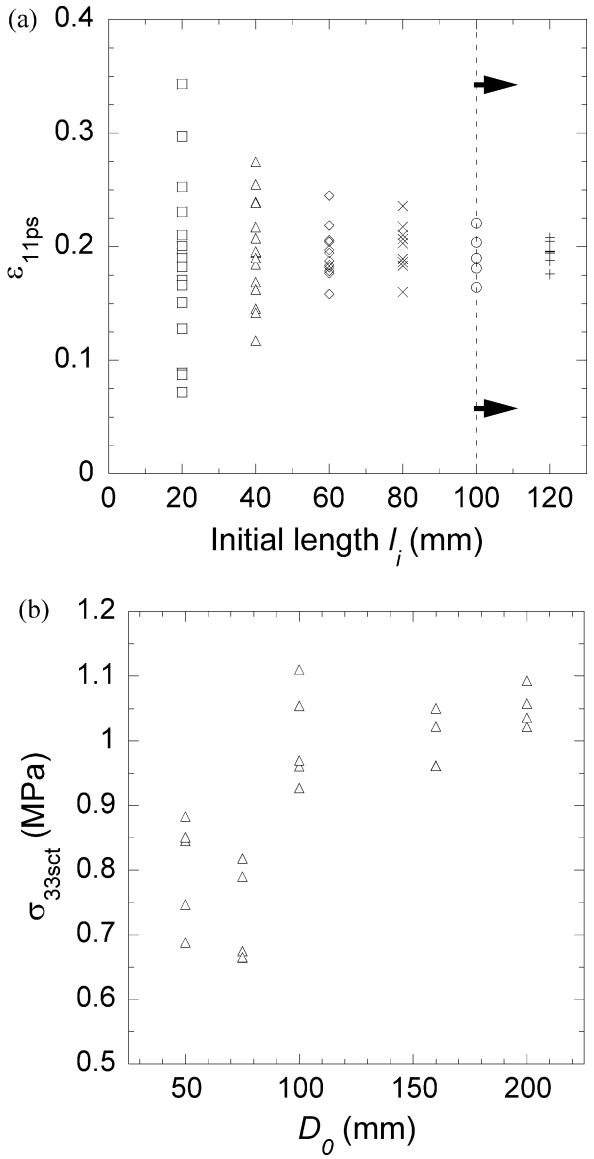

Fig. 3. (a) Plane strain compression, influence of l_i on ε_{33ps} ($\phi = 10.8\%$, $D_{33sc} = 0.01\ s^{-1}$), and (b) simple compression, influence of D_0 on stress levels ($\phi = 14.7\%$, $D_{33sc} = 0.01\ s^{-1}$).

volume fraction ϕ, n^{ϕ} is constant in the tested strain rate range. In the case of plane strain compression, the axial stress σ_{33pst} and the transverse stress σ_{22pst} are also power-law functions of D_{33ps}, as shown in Fig. 4c and d:

$$\sigma_{33pst} = \eta_{33ps}^{\phi} \left(\frac{D_{33ps}}{D_0} \right)^{n^{\phi}-1} D_{33ps} \tag{7}$$

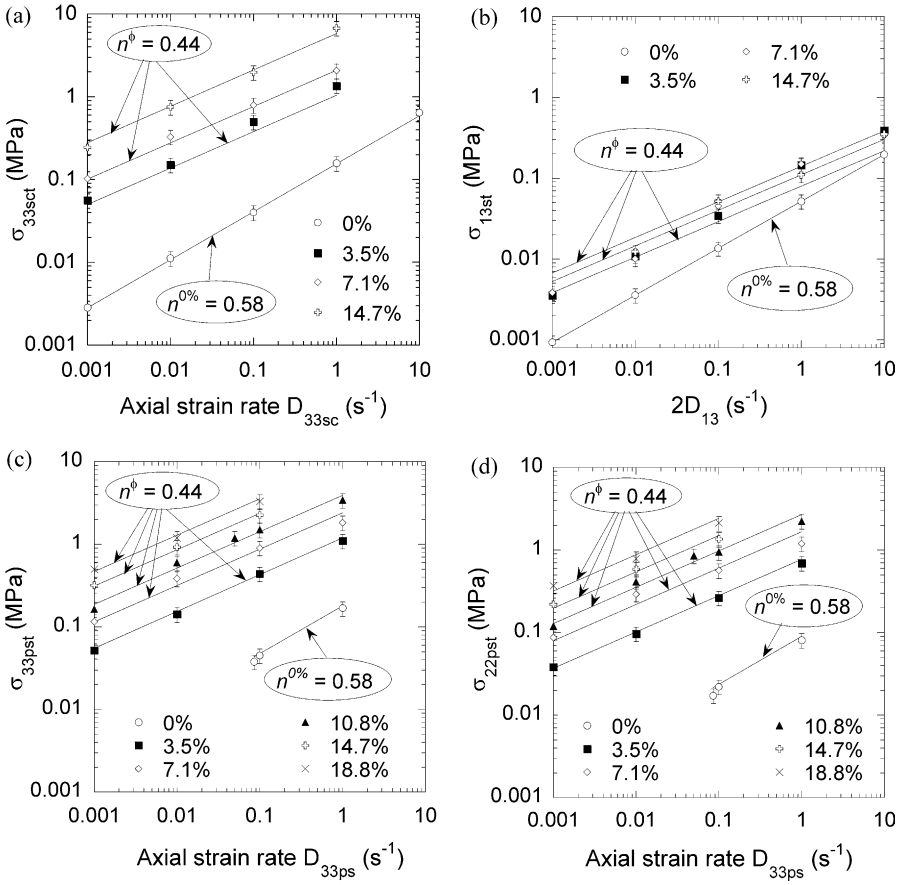

Fig. 4. Influence of the strain rate on stress levels for various fiber contents in (a) simple compression, (b) shear, (c) and (d) plane strain compression.

$$\sigma_{22pst} = \eta^{\phi}_{22ps}\left(\frac{D_{33ps}}{D_0}\right)^{n^{\phi}-1} D_{33ps} \tag{8}$$

A first important experimental result is that the power law exponent n^{ϕ} appearing in Eq. (6)–(8) does not depend on the mechanical loading (*sc* or *ps*). It is also of great interest to mention that the last noticing still applies for shear tests performed previously on the same SMC (Le Corre et al., in press), since the threshold shear stress σ_{13st} was shown to be a power law function of the shear strain rate $\dot{\gamma}_{13}$, with an identical power law exponent (see Fig. 4b):

$$\sigma_{13st} = 2\eta^{\phi}_{13s}\left(\frac{2D_{13}}{D_0}\right)^{n^{\phi}-1} D_{13} \tag{9}$$

3.3. Influence of the fiber volume fraction ϕ

The increase of the fiber volume fraction strongly affects the SMC rheology:

- The power law exponent coefficient n^{ϕ} equals 0.58 in the case of the paste ($\phi = 0\%$) and 0.44 for the rest of the tested fiber volume fractions ($\phi \geqslant 3.5\%$). These values are consistent with previous experimental results (Lee et al., 1981; Kim et al., 1992, 1997) and underline the "shear thinning" behavior of the paste and of the SMC, a typical effect observed in polymers (Ward, 1979; Khan and Haoyue, 2001).
- In Fig. 5a, dimensionless ratios $\eta^{\phi}_{33sc}/\eta^{0\%}_{33ps}$, $\eta^{\phi}_{33ps}/\eta^{0\%}_{33ps}$ and $\eta^{\phi}_{22ps}/\eta^{0\%}_{33ps}$ were plotted as functions of ϕ ($\eta^{0\%}_{33ps} = 0.18$ MPa). Whatever the imposed strain rates and the mechanical loading (*sc* or *ps*) are, these ratios are increasing functions of the fiber volume fraction. Second order polynomial functions were used to fit these variations (full lines in Fig. 5a):

$$\frac{\eta^{\phi}_{33sc}}{\eta^{0\%}_{33ps}} = 0.86 + 86\ \phi + 860\ \phi^2 \ \text{in simple compression}, \tag{10}$$

$$\frac{\eta^{\phi}_{33ps}}{\eta^{0\%}_{33ps}} = 1 + 98\ \phi + 980\ \phi^2 \ \text{in plane strain compression}, \tag{11}$$

$$\frac{\eta^{\phi}_{22ps}}{\eta^{0\%}_{33ps}} = 0.5 + 67\ \phi + 670\ \phi^2 \ \text{in plane strain compression}. \tag{12}$$

- Based on previous experiments (Le Corre et al., in press), the dimensionless ratio $\eta^{\phi}_{13s}/\eta^{0\%}_{33ps}$ was also plotted in Fig. 5a and fitted using a first order polynomial function:

$$\frac{\eta^{\phi}_{13s}}{\eta^{0\%}_{33ps}} = 0.33 + 3\ \phi \ \text{in shear}. \tag{13}$$

- As shown in Fig. 5b, the experimental stress ratio $\sigma_{33pst}/\sigma_{22pst}$ was also calculated for each fiber volume fraction. According to Eqs. (7) and (8), this ratio is not strain rate dependent and equals $\eta^{\phi}_{33ps}/\eta^{\phi}_{22ps}$. With the help of Eqs. (10) and (11), one obtains:

$$\frac{\sigma_{33pst}}{\sigma_{22pst}} = \frac{\eta^{\phi}_{33ps}}{\eta^{\phi}_{22ps}} = \frac{1 + 98\ \phi + 980\ \phi^2}{0.5 + 67\ \phi + 670\ \phi^2}. \tag{14}$$

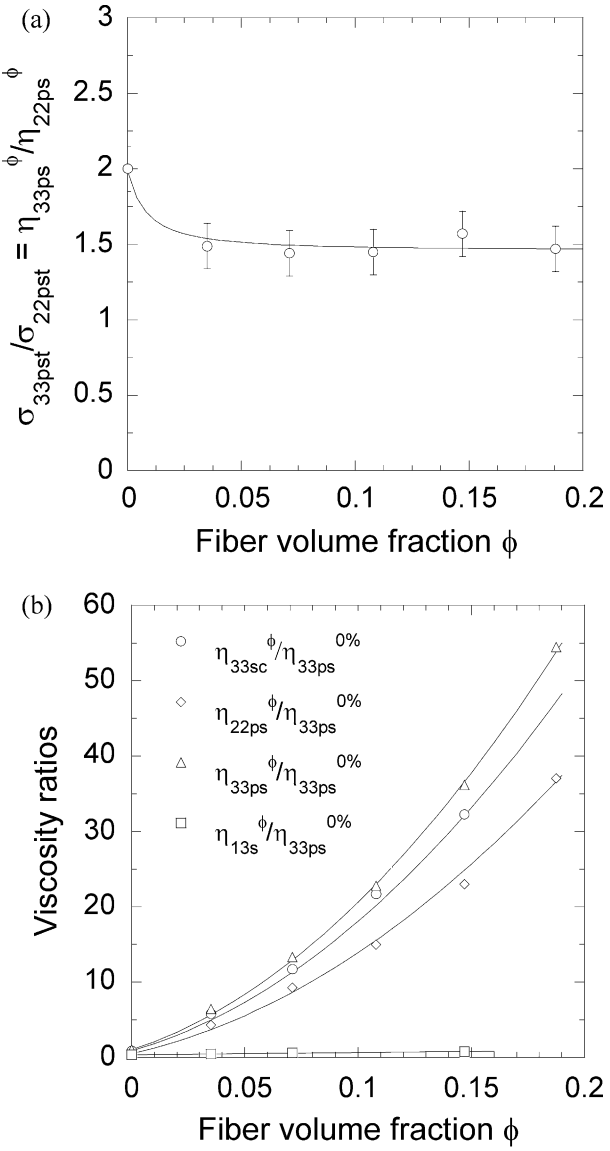

Fig. 5. Influence of the fiber content on (a) the dimensionless ratios (10)–(13) and (b) the stress ratio (14).

4. A viscous transverse isotropic model for the SMC

4.1. Formulation

Based on experimental results presented above, we propose in this section a set of constitutive equations to model the rheological behavior of SMC. A continuum

approach is here adopted. Due to the presence of fibers, the continuum assumption is valid only for sufficiently large SMC elementary volumes, as reported by experimental results of Section 3.1. Moreover, SMC, i.e. the paste and the fibers, are regarded as forming a one-phase and homogeneous medium from a macroscopic point of view.

Fibers induce preferred directions in SMC. For this reason, it seems interesting to account for such a microstructure in the continuum model. As a first approximation, fibers will be considered as evenly and randomly distributed in the plane of the sheets during the whole SMC deformation. This assumption, strictly valid at the beginning of the deformation, leads to define a single privileged direction perpendicular to the plane of the sheets and to consider SMC as transversely isotropic materials. The privileged direction is characterized by a unit vector $\mathbf{e}$ normal to the plane of the sheet or by a structural symmetric second order tensor $\mathbf{M}$ defined as:

$$\mathbf{M} = \mathbf{e} \otimes \mathbf{e}. \tag{15}$$

Moreover, SMC are assumed to be incompressible materials so that

$$\mathbf{D} : \boldsymbol{\delta} = 0 \tag{16}$$

where $\mathbf{D}$ is the strain rate tensor and $\boldsymbol{\delta}$ is the identity tensor. Thus, the stress tensor $\boldsymbol{\sigma}$ is split into two parts:

$$\boldsymbol{\sigma} = -p_0 \ \boldsymbol{\delta} + \boldsymbol{\sigma}^v \tag{17}$$

where p_0 is an arbitrary pressure, and $\boldsymbol{\sigma}^v$ is the extra stress tensor.

To further simplify the model, the extra stress tensor $\boldsymbol{\sigma}^v$ is assumed to be of purely viscous nature. It only depends on the strain rate tensor $\mathbf{D}$ and on the fiber volume fraction ϕ. Doing so, the resulting model will therefore only focus on threshold stresses recorded during the experiments. A more general approach would be to consider the rheological behavior of SMC as deformation history dependent. Models of this type could be formulated, but the additional complexity that would be involved does not seem to be justified at the present stage. Hence, it can be inferred from standard results of the theory of tensor functions representation (Boehler, 1987; Betten, 1988) that the irreducible canonical form of $\boldsymbol{\sigma}^v$ is

$$\begin{aligned} \boldsymbol{\sigma}^v = {} & \beta_0 \ \boldsymbol{\delta} + \beta_1 \ \mathbf{M} + \beta_2 \ \mathbf{D} + \beta_3(\mathbf{M}\cdot\mathbf{D} + \mathbf{D}\cdot\mathbf{M}) + \beta_4 \ \mathbf{D}\cdot\mathbf{D} \\ & + \beta_5 \ (\mathbf{M}\cdot\mathbf{D}\cdot\mathbf{D} + \mathbf{D}\cdot\mathbf{D}\cdot\mathbf{M}) \end{aligned} \tag{18}$$

where coefficients β_i may depend on ϕ and on the orthotropic strain rate invariants

$$\mathbf{D} : \mathbf{D}, \quad (\mathbf{D}\cdot\mathbf{D}) : \mathbf{D}, \quad \mathbf{M} : \mathbf{D} \quad \text{and} \quad (\mathbf{D}\cdot\mathbf{M}) : \mathbf{D} \tag{19}$$

Within such a general framework, the viscous stress tensor $\boldsymbol{\sigma}^v$ is now supposed to be the gradient of a viscous potential Ω with respect to the strain rate tensor $\mathbf{D}$ (Nguyen et al., 1994; Martin et al., 1997, 1999). To fulfill the second principle of

thermodynamics, Ω must be positive, convex, and $\frac{\partial\Omega}{\partial\mathbf{D}}=0$ must be zero when $\mathbf{D}=0$. We further assume that Ω is expressed by means of an equivalent strain rate D_{eq}, scalar function of the strain rate tensor $\mathbf{D}$ and of the fiber volume fraction ϕ:

$$\Omega=\Omega\big(D_{\mathrm{eq}}(\mathbf{D},\phi),\phi\big). \tag{20}$$

This implies:

$$\boldsymbol{\sigma}^{v}=\frac{\partial\Omega}{\partial\mathbf{D}}=\frac{\partial\Omega}{\partial D_{\mathrm{eq}}}\frac{\partial D_{\mathrm{eq}}}{\partial\mathbf{D}}=\sigma_{\mathrm{eq}}\frac{\partial D_{\mathrm{eq}}}{\partial\mathbf{D}}, \tag{21}$$

where σ_{eq} is the equivalent stress associated with D_{eq}. The proposed form of D_{eq} is similar to the one used by Meyssonier et al. (2001) to model the anisotropic viscous behavior of polar ice:

$$\begin{aligned}&D_{\mathrm{eq}}^{2}=\alpha_0\big(\mathbf{D}:\mathbf{D}+\alpha_1(\mathbf{M}:\mathbf{D})^{2}+\alpha_2(\mathbf{D}\cdot\mathbf{M}):\mathbf{D}\big)\\&\quad\text{with}\ \ \alpha_0=\frac{2}{1+2H^{\phi}},\quad \alpha_1=\left(1+H^{\phi}-2\frac{1+2H^{\phi}}{3L^{\phi}}\right)\\&\quad\text{and}\quad \alpha_2=2\left(\frac{1+2H^{\phi}}{3L^{\phi}}-1\right)\end{aligned} \tag{22}$$

and where $H^{\phi}>-1/2$ and $L^{\phi}>0$ are rheological functions that characterize the transverse isotropy. In this work, these rheological functions depend on the fiber volume fraction ϕ and equal 1 in the case of isotropy. Accounting for Eqs. (21) and (22), the general form of the extra stress tensor (18) is now reduced to

$$\boldsymbol{\sigma}^{v}=\alpha_0\ \ \eta_{eq}\left(\mathbf{D}+\alpha_1(\mathbf{M}:\mathbf{D})\mathbf{M}+\frac{1}{2}\alpha_2(\mathbf{M}\cdot\mathbf{D}+\mathbf{D}\cdot\mathbf{M})\right) \tag{23}$$

where η_{eq} is the equivalent viscosity defined as

$$\sigma_{\mathrm{eq}}=\eta_{\mathrm{eq}}\ \ D_{\mathrm{eq}} \tag{24}$$

The deviatoric stress tensor $\mathbf{s}$ is then

$$\mathbf{s}=\boldsymbol{\sigma}-\frac{\boldsymbol{\sigma}:\boldsymbol{\delta}}{3}\boldsymbol{\delta}=\boldsymbol{\sigma}^{v}-\frac{2\ \ \eta_{\mathrm{eq}}}{3}\frac{H^{\phi}-1}{1+2H^{\phi}}(\mathbf{M}:\mathbf{D})\boldsymbol{\delta}. \tag{25}$$

It can be shown that Eqs. (22)–(25), together with the viscous dissipation P_{dis}

$$P_{\mathrm{dis}}=\mathbf{s}:\mathbf{D}=\sigma_{\mathrm{eq}}\ \ D_{\mathrm{eq}}, \tag{26}$$

enable to write the equivalent stress σ_{eq} as

$$\sigma_{\mathrm{eq}}^2 = \frac{1}{2}\left(\left(1+2H^{\phi}\right)\mathbf{s}:\mathbf{s} + \left(5+H^{\phi}-6L^{\phi}\right)(\mathbf{M}:\mathbf{s})^2 - 2\left(1+2H^{\phi}-3L^{\phi}\right)(\mathbf{s}\cdot\mathbf{M}):\mathbf{s}\right) \tag{27}$$

During the present experiments, $\mathbf{M}$ was time independent and $\mathbf{e}=\mathbf{e}_3$. In that particular case, it can be shown that the form of σ_{eq}, expressed in the Cartesian reference frame $(\mathbf{e}_1,\mathbf{e}_2,\mathbf{e}_3)$, is very close to the form of the yield stress proposed by Hill (1950) for plastic metallic materials displaying an $\mathbf{e}_3$-transverse isotropy, i.e

$$\begin{aligned} 2\ \sigma_{\mathrm{eq}}^2 = {} & H^{\phi}(\sigma_{11}-\sigma_{22})^2 + (\sigma_{22}-\sigma_{33})^2 + (\sigma_{33}-\sigma_{11})^2 \\ & + 6L^{\phi}\left(\sigma_{23}^2+\sigma_{31}^2\right) + 2\left(1+2H^{\phi}\right)\sigma_{12}^2 \end{aligned} \tag{28}$$

The last expression is also identical to the equivalent stress proposed by previous authors to model the rheological behavior of SMC (Kim et al., 1992). However, thanks to the use of the structural tensor $\mathbf{M}$, the present tensorial formulation, i.e. Eqs. (20)–(27) is frame independent.

Following experimental results presented in Section 3.2, it may be convenient to define the equivalent viscosity η_{eq} as a power law function of D_{eq}:

$$\eta_{\mathrm{eq}} = \eta_{0\mathrm{eq}}^{\phi}\left(\frac{D_{\mathrm{eq}}}{D_0}\right)^{n_{\mathrm{eq}}^{\phi}-1}, \tag{29}$$

where $\eta_{0\mathrm{eq}}^{\phi}$ is a viscosity determined from the condition that D_{eq} equals a characteristic strain rate D_0 ($=1\ \mathrm{s}^{-1}$ in this work) and where n_{eq}^{ϕ} is the power law exponent. To further fit experimental results given in section 3.3, $\eta_{0\mathrm{eq}}^{\phi}$ and n_{eq}^{ϕ} may be functions of the fiber volume fraction ϕ.

At last, in the Cartesian reference frame ($\mathbf{e}_1$, $\mathbf{e}_2$, $\mathbf{e}_3$), predictions of the model in simple compression [*sc*, Eq. (1)] and plane strain compression [*ps*, Eq. (2)] and shear (*s*) lead respectively to the following set of useful equations:

$$\sigma_{33sc} = \eta_{0\mathrm{eq}}^{\phi}|D_{33sc}|^{n_{\mathrm{eq}}^{\phi}-1}D_{33sc} \tag{30}$$

$$\sigma_{33ps} = \eta_{0\mathrm{eq}}^{\phi}\left(2\frac{1+H^{\phi}}{1+2H^{\phi}}\right)^{\frac{n_{\mathrm{eq}}^{\phi}+1}{2}}\left|D_{33ps}\right|^{n_{\mathrm{eq}}^{\phi}-1}D_{33ps} \tag{31}$$

$$\sigma_{22ps} = \eta_{0\mathrm{eq}}^{\phi}\left(1+H^{\phi}\right)^{\frac{n_{\mathrm{eq}}^{\phi}-1}{2}}\left(\frac{2}{1+2H^{\phi}}\right)^{\frac{n_{\mathrm{eq}}^{\phi}+1}{2}}\left|D_{33ps}\right|^{n_{eq}^{\phi}-1}D_{33ps} \tag{32}$$

$$\frac{\sigma_{33ps}}{\sigma_{22ps}} = 1+H^{\phi} \tag{33}$$

$$\sigma_{13s} = \eta_{0\mathrm{eq}}\frac{(2D_{13})^{n_{\mathrm{eq}}^{\phi}}}{(3L^{\phi})^{(n_{\mathrm{eq}}^{\phi}+1)/2}} \tag{34}$$

4.2. Determination of constitutive parameters

In the rheological model briefly introduced in the previous subsection, four parameters are involved, i.e. the viscosity $\eta^{\phi}_{0\mathrm{eq}}$, the power law exponent n^{ϕ}_{eq} and the two anisotropic rheological functions H^{ϕ} and L^{ϕ}.

As revealed by Eqs. (30)–(33), plane strain compression and simple compression experiments are useful to determine $\eta^{\phi}_{0\mathrm{eq}}$, n^{ϕ}_{eq} and H^{ϕ}. Given a fiber volume fraction ϕ, two methods of determination are available.

- The first method consists in carrying out a first set of simple compression experiments at various axial strain rates to find out $\eta^{\phi}_{0\mathrm{eq}}$ and n^{ϕ}_{eq}. It follows from Eq. (30) that

$$\eta^{\phi}_{0\mathrm{eq}} = \eta^{\phi}_{33sc} \quad \text{and} \quad n^{\phi}_{\mathrm{eq}} = n^{\phi}. \tag{35}$$

  Then performing one plane strain compression experiment on one different SMC specimen and combining Eqs. (30) and (31) to obtain

$$H^{\phi} = \frac{1}{2}\frac{\left(\sigma_{33pst}\right)^{\frac{2}{n^{\phi}+1}} - 2\left(\eta^{\phi}_{33sc}\ D^{n^{\phi}}_{33ps}\right)^{\frac{2}{n^{\phi}+1}}}{\left(\eta^{\phi}_{33sc}\ D^{n^{\phi}}_{33ps}\right)^{\frac{2}{n^{\phi}+1}} - \left(\sigma_{33pst}\right)^{\frac{2}{n^{\phi}+1}}}, \tag{36}$$

  it appears that a unique measurement of the axial stress σ_{33pst} during the plane strain compression experiment is sufficient to get H^{ϕ}. However, our experimental results display relative errors $[\Delta\sigma_{33pst}/\sigma_{33pst}]$, $[\Delta\eta^{\phi}_{33sc}/\eta^{\phi}_{33sc}]$, $[\Delta n^{\phi}/n^{\phi}]$ and $[\Delta D_{33ps}/D_{33ps}]$ of about ± 20, ± 25, ± 10 and $\pm$ 5%, respectively. According to Eq. (36) and depending on the testing conditions (i.e. ϕ and D_{33ps}) used to estimate H^{ϕ}, this may induce unacceptable relative error for H^{ϕ} ranging between $\pm$ 85% and $\pm$ 190, 000% (!) (see Appendix A for details). For that reason, this first method has to be prohibited.
- Thanks to the measurement of the transverse stress σ_{22pst} during our plane strain compression experiments, a second method to determine $\eta^{\phi}_{0\mathrm{eq}}$, n^{ϕ}_{eq} and H^{ϕ} using a unique set of plane strain compression experiments is now proposed. Firstly, combined with Eq. (34), a plane strain compression experiment is performed to determine H^{ϕ}:

$$H^{\phi} = \frac{\sigma_{33pst}}{\sigma_{22pst}} - 1 \tag{37}$$

Then, a set of plane strain compression experiments performed at various axial strain rates together with Eq. (31) gives the values of $\eta^{\phi}_{0\mathrm{eq}}$ and n^{ϕ}_{eq}:

$$n^{\phi}_{\mathrm{eq}} = n^{\phi} \quad \text{and} \quad \eta^{\phi}_{0\mathrm{eq}} = \eta^{\phi}_{33ps}\left(2\frac{1+H^{\phi}}{1+2H^{\phi}}\right)^{-\frac{n^{\phi}+1}{2}} \tag{38}$$

Experimental results give relative errors $[\Delta\eta^{\phi}_{33ps}/\eta^{\phi}_{33ps}]$, $[\Delta n^{\phi}/n^{\phi}]$ of about $\pm 25\%$, and $\pm 10\%$, respectively. The inaccuracy of the experimental stress ratio $\sigma_{33pst}/\sigma_{22pst}$ was estimated to be of order $\pm 10\%$. According to Eq. (37), this will induce a variation $[\Delta H^{\phi}/H^{\phi}]$ of about $\pm 30\%$. As a consequence and thanks to Eq. (38)b, a relative error for $\eta^{\phi}_{0\mathrm{eq}}$ of about $\pm 30\%$ is expected (see Appendix B for details). Thus, the second method leads to fairly reasonable errors on the determination of constitutive parameters.

Constitutive parameters $\eta^{\phi}_{0\mathrm{eq}}$, n^{ϕ}_{eq} and H^{ϕ} were therefore determined using the second method. According to experimental results [Eq. (14)] and to the model prediction [Eq. (37)], H^{ϕ} is a function of the fiber volume fraction:

$$H^{\phi} = \frac{1 + 98\ \phi + 980\ \phi^2}{0.5 + 67\ \phi + 670\ \phi^2} - 1. \tag{39}$$

Experimental results also lead to choose a power law exponent n^{ϕ}_{eq} such as

$$\begin{aligned} &n^{\phi}_{\mathrm{eq}} = 0.58 \text{ for } \phi = 0 \text{ and} \\ &n^{\phi}_{\mathrm{eq}} = 0.44 \text{ for } \phi = 3.5,\ 7.1,\ 10.8,\ 14.7 \text{ and } 18.8\% \end{aligned} \tag{40}$$

Based on Eq. (38)b, the viscosity $\eta^{\phi}_{0\mathrm{eq}}$ is given by

$$\eta^{\phi}_{0\mathrm{eq}} = 0.18\left(1 + 98\ \phi + 980\ \phi^2\right)\left(2\frac{1 + H^{\phi}}{1 + 2H^{\phi}}\right)^{-\frac{n^{\phi}+1}{2}}. \tag{41}$$

To end with, given the values of $\eta^{\phi}_{0\mathrm{eq}}$, n^{ϕ}_{eq} and H^{ϕ} [Eqs. (39)–(41)], a shear experiment combined with Eq. (34) lead to the determination of the last rheological function L^{ϕ}:

$$L^{\phi} = \frac{1 + 2H^{\phi}}{6(1 + H)}\left(\frac{1 + 98\ \phi + 980\ \phi^2}{0.33 + 3\ \phi}\right)^{\frac{2}{n^{\phi}+1}} \tag{42}$$

To check the good agreement between experimental results of shear, simple compression and plane strain compression tests and the proposed rheological model, the equivalent strain rate D_{eq} defined in Eq. (22) as well as the equivalent stress σ_{eq} given in Eq. (27) were estimated thanks to experimental results for all the tested strain rates and fiber volume fractions, as shown in Fig. 6. The full lines also plotted in this figure correspond to the predictions of the model given by Eqs. (24) and (29), n^{ϕ}_{eq} and $\eta^{\phi}_{0\mathrm{eq}}$ being respectively given by Eqs. (40) and (41). As evident in this figure, a fairly good agreement is found between the model and the experiments.

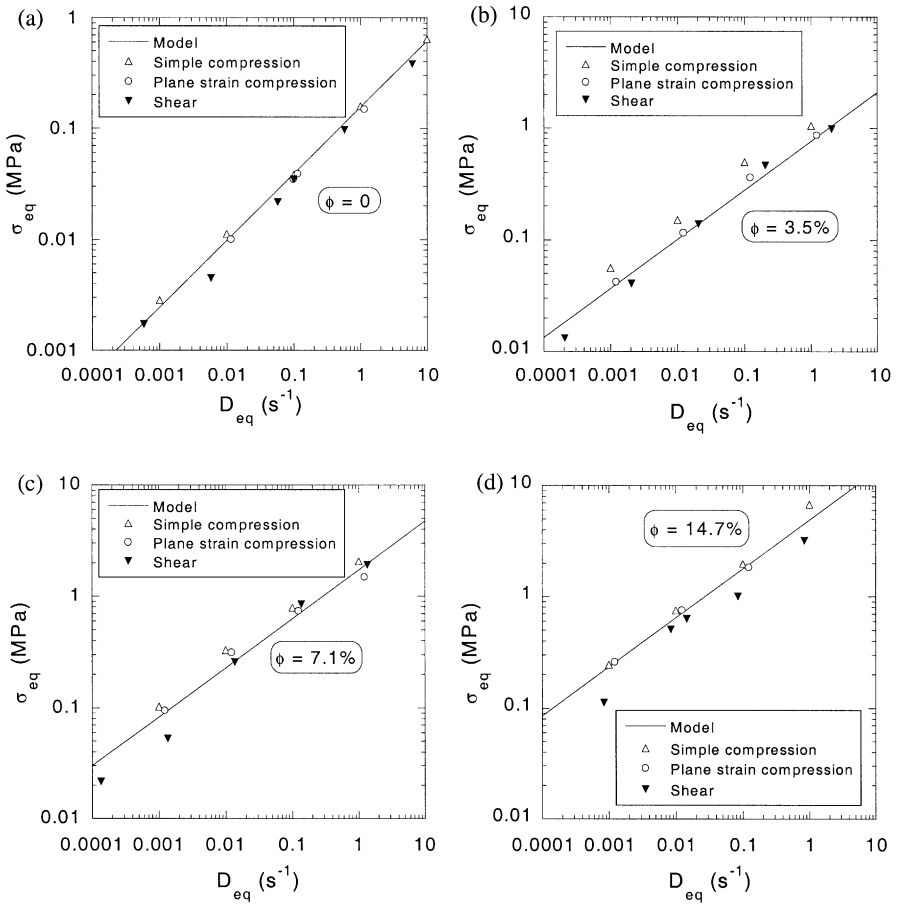

Fig. 6. Comparison between experimental results and the prediction of the proposed model, (a) $\phi = 0$, (b) $\phi = 3.5\%$, (c) $\phi = 7.1\%$, (d) $\phi = 14.7\%$.

5. Conclusion

To improve the knowledge of the rheology of SMC during compression molding, a specific rheometer was designed, allowing to perform homogeneous experiments on SMC specimen under various mechanical loading, strain rates and fiber contents. Results underlined the key role played both by the strain rate and the fiber content. Stress levels were proved to be power law functions of the strain rate, leading to a strong shear thinning behavior. They were also proved to be increasing functions of the fiber content. Increasing the fiber content also lead to enhance the anisotropy of SMC. A rather simple non linear viscous and transversely isotropic model was then proposed and used to fit stress levels recorded during the experiments. This model which gives reasonable agreement with experimental data, accounts for the main

features of SMC rheology, and can be easily implemented in commercial simulation code for compression molding.

Acknowledgements

S. Le Corre is grateful to Schneider Electric for its financial support. We would also like to thank our other industrial partners, Renault and Inoplast, together with the Région Rhône-Alpes.

Appendix A. Relative error for H^{Φ} induced with the first method to determine the parameter of the anisotropic viscous model

According to Eq. (36), the error ΔH^{ϕ} is expressed as:

$$\Delta H^{\phi} = \left|\frac{A}{v} + Bu\right|\Delta\sigma_{33pst} + \left|\frac{C}{v} + Du\right|\Delta\eta^{\phi}_{33sc} + \left|\frac{E}{v} + Fu\right|\Delta D_{33ps} + \frac{\left|\frac{\partial u}{\partial n^{\phi}}v - u\frac{\partial v}{\partial n^{\phi}}\right|}{v^2}\Delta n^{\phi}$$

using the notations:

$$u = \frac{1}{2}\left(\frac{\sigma_{33pst}}{\eta^{\phi}_{33sc}D^{n^{\phi}}_{33ps}}\right)^{\frac{2}{1+n^{\phi}}} - 1, \qquad v = 1 - \left(\frac{\sigma_{33pst}}{\eta^{\phi}_{33sc}D^{n^{\phi}}_{33ps}}\right)^{\frac{2}{1+n^{\phi}}},$$

$$A = \frac{1}{(1+n^{\phi})\eta^{\phi}_{33sc}D^{n^{\phi}}_{33ps}}\left(\frac{\sigma_{33pst}}{\eta^{\phi}_{33sc}D^{n^{\phi}}_{33ps}}\right)^{\left(\frac{1-n^{\phi}}{1+n^{\phi}}\right)}, \qquad B = -\frac{2}{v^2}A,$$

$$C = -\frac{1}{\eta^{\phi 2}_{33sc}}A, \qquad D = \frac{2\sigma_{33pst}}{\eta^{\phi 2}_{33sc}v^2}A, \qquad E = -\frac{n^{\phi}\sigma_{33pst}}{D_{33ps}}A, \qquad F = \frac{2n^{\phi}\sigma_{33pst}}{v^2}A,$$

$$a = 2\left(\ln\sigma_{33pst} - \ln\eta_{0eq}\right), \qquad b = 2\ln D_{33ps},$$

$$\frac{\partial u}{\partial n^{\phi}} = -\frac{(a+b)}{2(1+n^{\phi})^2}e^{\left(\frac{a}{1+n^{\phi}}\right)}e^{-\left(\frac{n^{\phi}b}{1+n^{\phi}}\right)}, \qquad \frac{\partial v}{\partial n^{\phi}} = \frac{1}{2}\left(\frac{\partial u}{\partial n^{\phi}}\right).$$

To estimate the relative error $[\Delta H^{\phi}/H^{\phi}]$, one has to first take into account the following approximations deduced from experiments: $[\Delta\sigma_{33pst}/\sigma_{33pst}] \approx \pm 20\%$,

$[\Delta\eta^{\phi}_{33sc}/\eta^{\phi}_{33sc}]\approx\pm 25\%$, $[\Delta n^{\phi}/n^{\phi}]\approx\pm 10\%$ and $[\Delta D_{33ps}/D_{33ps}]\approx\pm 5\%$. ΔH^{ϕ} was then calculated for all our experimental data. In one of the best cases, i.e. for $\phi=0.148$ and $D_{33ps}=0.01\text{s}^{-1}$ ($\sigma_{33pst}=0.927$ MPa and $\eta^{\phi}_{33sc}=5.8$ MPa.s), ΔH^{ϕ} is found to equal ± 1.7. In one of the worst cases, i.e. for $\phi=0.035$ and $D_{33ps}=1\text{s}^{-1}$ ($\sigma_{33pst}=1.05$ MPa and $\eta^{\phi}_{33sc}=1.04$ MPa.s), ΔH^{ϕ} is found to equal ± 1900. Thanks to the measurements of σ_{22pst} during our experiments, we know that H^{ϕ} ranges between 2 and 1 (with an accuracy of $\pm 30\%$). Consequently, depending on the testing conditions chosen to estimate H^{ϕ}, the first method can yield to a relative error $[\Delta H^{\phi}/H^{\phi}]$ that ranges between ± 85 and $\pm 190\,000\%$.

Appendix B. Relative error for $\eta^{\phi}_{0\text{eq}}$ induced by the second method

According to Eq. (38)b, the error $\Delta\eta^{\phi}_{0\text{eq}}$ is expressed as:

$$\Delta\eta^{\phi}_{0\text{eq}} = A'\Delta\eta^{\phi}_{33ps} + B'\Delta H^{\phi} + C'\Delta n^{\phi}$$

using the notations:

$$A' = \left(2\frac{1+H^{\phi}}{1+2H^{\phi}}\right)^{-\left(\frac{n^{\phi}+1}{2}\right)}, \qquad B' = \frac{\eta^{\phi}_{33ps}\left(1+n^{\phi}\right)}{(1+2H^{\phi})^{2}\left(2\frac{1+H^{\phi}}{1+2H^{\phi}}\right)^{\left(\frac{n^{\phi}+3}{2}\right)}}$$

$$\text{and} \qquad C' = \eta^{\phi}_{33ps}\left|-\frac{1}{2}\ln\left(\frac{2\left(1+H^{\phi}\right)}{(1+2H^{\phi})}\right)\right|\left(2\frac{1+H^{\phi}}{1+2H^{\phi}}\right)^{-\left(\frac{n^{\phi}+1}{2}\right)}$$

Whatever experimental values of H^{ϕ}, η^{ϕ}_{33ps}, and n^{ϕ}, and accounting for $[\Delta H^{\phi}/H^{\phi}]\approx\pm 10\%$, $[\Delta\eta^{\phi}_{33ps}/\eta^{\phi}_{33ps}/\eta^{\phi}_{33ps}]\approx\pm 25\%$ and $[\Delta n^{\phi}/n^{\phi}]\approx\pm 10\%$ of about $\pm 25\%$, the relative error $[\Delta\eta^{\phi}_{0\text{eq}}/\eta^{\phi}_{0\text{eq}}]$ is always below $\pm 30\%$.

References

Barone, M.R., Caulk, D.A., 1985. Kinematics of flow of sheet molding compounds. Polymer Composites 6 (2), 105–109.

Barone, M.R., Caulk, D.A., 1986. A model for the flow of a chopped reinforced polymer compound in compression molding. Journal of Applied Mechanics 53, 361–371.

Batchelor, G.K., 1970. The stress system in a suspension of force-free particles. J. Fluid. Mech. 41 (3), 545–570.

Betten, J., 1988. Applications of tensor functions to the formulation of yield criteria for anisotropic materials. Int. J. Plasticity 4, 29–46.

Boehler, J.-P., 1987. Applications of tensor functions in solid mechanics. In: Boehler, J.-P. (Ed.), CISM Courses and Lectures, No. 292. Springer-Verlag, Wien, NY.

Castro, J.M., Griffith, R.M., 1989. Sheet molding compound compression-molding flow. Polymer Engineering and Science 29 (10), 632–637.

Castro, J.M., Tomlinson, G., 1990. Predicting molding forces in SMC compression molding. Polymer Engineering and Science 30 (24), 1568–1573.

Hill, R., 1950. Mathematical Theory of Plasticity. Oxford University Press, Oxford, UK.

Khan, A., Haoyue, Z., 2001. Finite deformation of a polymer: experiments and modeling. Int. J. Plasticity 17 (9), 1167–1188.

Kim, J., Shiau, Y.C., Lee James, L., Im, Y.T., 1992. Compression molding simulation of chopped fiber reinforced polymeric composites in plate-rib type geometry. Polymer Composites 13 (2), 97–107.

Kim, K.-T., Jeong, J.-H., Im, Y.-T., 1997. Effect of molding parameters on compression molded sheet molding compounds parts. J. Mater. Process. Technol. 67, 105–111.

Le Corre S., Orgéas L., Favier D., Tourabi A., Maazouz A., Venet C., in press. Shear and compression behavior of sheet molding compounds. Composite Science and Technology.

Lee, L.J., Marker, L.F., Griffith, R.M., 1981. The rheology and mold flow of polyester sheet molding compound. Polymer Composites 2 (4), 209–218.

Lee, C.C., Folgar, F., Tucker, C.L., 1984. Simulation of compression molding for fiber-reinforced thermosetting polylmers. Polymer Composites 106, 114–125.

Lin, C.M., Weng, C.I., Ho, C.T., 1997. Anisotropy in sheet molding compounds during compression molding. Polymer Composites 18 (5), 613–622.

Lin, C.M., Weng, C.I., 1999. Simulation of compression molding for sheet molding compound considering the anisotropic effect. Polymer Composites 20 (1), 98–113.

Marker, L.F., Ford, B., 1977. Flow and curing behavior of SMC during molding. Modern Plastics 54, 64–70.

Martin, C.L., Favier, D., Suéry, M., 1997. Viscoplastic behaviour of porous metallic materials saturated with liquid. Part I : constitutive equations. Int. J. Plasticity 13 (3), 215–235.

Martin, C.L., Favier, D., Suéry, M., 1999. Fracture behaviour in tension of viscoplastic porous metallic materials saturated with liquid. Int. J. Plasticity 15 (10), 981–1008.

Michaeli, W., Mahlke, M., Osswald, T.A., 1990. Analyse und Messung des Fliessens von SMC mit einem Pressrheometer. Kunstoffe 80, 70–74.

Meyssonnier J., Duval P., Gagliardini O., Philip A., 2001. Constitutive modelling and flow simulation of anisotropic polar ice. In: Straughan, Greve, Ehrentraut, Wang (Eds.), Continuum Mechanics and Applications in Geophysics and the Environment. Springer, pp. 250–275.

Nguyen, T.G., Favier, D., Suéry, M., 1994. Theoretical and experimental study of the isothermal mechanical behavior of alloys in the semi-solid state. Int. J. Plasticity 10 (6), 663–693.

Scott, J.R., 1931. Theory and application of the parallel-plate plastimeter. Trans. Inst. Rubber Ind. 7, 169–186.

Silva-Nieto, R.J., Fisher, B.C., Birley, A.W., 1980. Predicting mold flow for unsaturated polyester resin sheet molding compounds. Polymer Composites 1 (1), 14–23.

Silva-Nieto, R.J., Fisher, B.C., Birley, A.W., 1981. Rheological characterization of unsaturated polyester resin sheet molding compounds. Polymer Engineering and Science 21 (8), 499–506.

Ward, I.M., 1979. Mechanical Properties of Solid Polymers. John Wiley & Sons, New York.

Xu, J., Kim, J., Ho, T., Lee, J.L., 1993. Compression molding of sheet molding compounds in plate-rib type geometry. Polymer Composites 14 (1), 51–58.